# Comparing Multi-Point Constraints in Nonlinear Modeling of a Two-Dimensional Beam

**Brennan Bahr[1], Benjamin J. Crapo[1], Matthew S. Allen[2], Raymond Joshua[3*]**

[1]Undergraduate Student, Brigham Young University, Department of Mechanical Engineering
[2]Professor, Brigham Young University, Department of Mechanical Engineering, matt.allen@byu.edu
[3]Senior Mechanical Engineer, Kansas City National Security Campus

**Abstract**

Full order finite element models are often too computationally expensive to be seen as a viable option for predicting the nonlinear dynamic response of systems with joints. To lower this cost, reduced-order modeling techniques have been developed that significantly decrease the time needed to predict the response of a system. The use of Multi-Point Constraints (MPCs), in conjunction with Hurty/Craig-Bampton reduction, can significantly lower the computational expense required. However, few works have investigated how this approach affects the accuracy of the model, as compared to a high-fidelity truth model. This work applies several types of MPCs to a benchmark model comprised of two cantilever beams with a frictional joint connecting their free ends. A two-dimensional model is used so that the quasi-static and dynamic response of a high-fidelity truth model can be computed and compared to that of the reduced models. The linearized modes of the reduced model are compared to those of the truth model, to see which spidering approaches produce the best accuracy. The models are then compared in terms of their ability to capture the amplitude dependent natural frequency and damping of the fundamental mode of the assembly.

**Keywords**: Iwan Joints, Friction, Nonlinear Joint, Model Updating

## 1 Introduction

Finite Element Analysis (FEA) has become essential in structural dynamics, enabling engineers to predict the dynamic response, and hence the loading in critical structural members, of complicated aerospace vehicles that are comprised of dozens of parts with intricate geometry. However, in practice these models are only predictive when the material properties are well known and the parts are rigidly bonded together. Interfaces introduce uncertainty as one must determine where to enforce contact and where the surfaces are bonded in the normal and tangential directions. The alternative, which would be to model the contact in detail while enforcing contact in the normal direction and Coulomb friction in the tangential direction, is extremely computationally expensive and not compatible with current workflows for structures such as launch vehicles, where the dynamic response must be computed for thousands of loading scenarios.

As a result, when structural dynamic models are created in industry, the geometry of the structure is simplified considerably and the joints between parts are replaced with some kind of spider or multipoint constraint (MPC). A good example of this was recently presented by Winkel et al. [1], who performed a study comparing the standard industry/NASA approach to other alternatives. When modeling a structure such as a launch vehicle, the typical practice is to use shell elements for each of the various parts, to simplify joints to a single node or small number of nodes by joining the nodes over an area with rigid bar elements (MPCs), and then to connect the joint nodes with springs or beam elements. These can then be tuned during model updating [2] to bring the modes of the model into agreement with measurements. When nonlinearity must be considered, the spring or beam elements can be replaced with nonlinear elements such as springs with Coulomb friction sliders [3].

It appears that the approach used in [3, 4] is actually quite common in industry, although there are not too many references to case studies, presumably because most of that work is kept in house. As a result, there are very few studies that explore how well this approach can capture the various types of nonlinearities that occur. This work is focused on the nonlinearity that arises due to macro-slip in a bolted joint. Along those lines, Segalman proposed the four parameter Iwan element [5] as a "whole joint element" that can be placed between two virtual nodes and used to capture micro- and macro-slip nonlinearity in an assembly. (Those virtual nodes are presumably connected to the rest of the structure through multi-point constraints.) The subsequent

*Honeywell Federal Manufacturing Technologies, LLC operates the Kansas City National Security Campus for the United States Department of Energy / National Nuclear Security Administration under Contract Number DE-NA0002839. UUR – NSC-614-6620

work at Sandia [6] validated many features of Segalman's Iwan element. However, it appears that Lacayo et al. [4, 7] was the first work to show that this approach was sufficient to allow the reduced model to bring the nonlinear features of several modes into agreement with measurements. Specifically, Lacayo et al. used MPC spiders to reduce the interface of a bolted assembly (the Brake-Reuss Beam [8]) to five pairs of virtual nodes. These were connected using Iwan elements. Lacayo et al. [4] found that the resulting model captured the low-amplitude, linear natural frequencies of several modes very well, and also captured the amplitude dependent effective natural frequency and damping of the first few modes with good accuracy. Singh et al. [9] later revisited that approach for the S4 Beam [10], showing that the same approach worked well to capture several linear modes of the structure and one mode that showed significant stick-slip nonlinearity.

Singh et al.'s work [9] explored the role of the spiders in more detail, varying the type of spider and the area that was connected by the spiders. They found that any of the spider methods or spider areas could produce a model that captured the linear natural frequencies of the first several modes of the structure, although each model had different spring constants between the virtual nodes. However, when checking the model's ability to capture the nonlinearity that was observed in experiments, he found that only rigid spiders (i.e. RBE2 or RBAR spiders in Nastran terminology) produced acceptable results. Those spiders allowed the reduced model to use less stiff springs between the parts, and this allowed the Iwan elements to more accurately capture the damping of the assembly. Singh et al.'s work compared a model to experimental data, and while there are certainly advantages to doing so, the true behavior of the system was only known to the resolution of the measurements.

Jewell et al. [11], proposed a 2D model that consists of two cantilever beams that are joined at their free ends due to a clamping force and Coulomb friction. The beams are modeled in two dimensions (plane strain), so the model is reasonably inexpensive to simulate and yet it can capture micro-slip behavior in detail. This work uses Jewell's model to explore the ability of reduced models with MPC spiders to capture the behavior of bolted joints. The detailed FEM is taken as the truth model, as it presumably captures the actual physics of the bolted interface. Then a reduced order model is created by simplifying the interface with various types of MPC spiders and then reducing the model using the Hurty/Craig-Bampton (HCB) method [12, 13]. Simulations of the truth model are used as experimental data and then the reduced model is updated using the approach in [4, 9] to see the extent to which the reduced model can capture the actual physics of the truth model.

This work uses the commercial FEA package Abaqus, which allows one to define spider constraints as kinematic (i.e. similar to Nastran RBE2) or continuum (i.e. Nastran RBE3) distributed, with the latter having additional options for how a force should be distributed from the parent node (virtual node in our case) to its children (uniform, linear, quadratic, or cubic) [14].

The next section briefly reviews the theoretical basis behind the modeling methods used here. Then the case studies are presented followed by the conclusions.

# 2 Theory

This work utilizes the Hurty/Craig-Bampton Method to reduce the size of the finite element model and then Quasi-Static Modal Analysis (QSMA) to quickly estimate the effective natural frequency and damping of the system. A brief overview of these methods is given in the following subsections.

## 2.1 Hurty-Craig/Bampton Method

The Hurty/Craig-Bampton method simplifies the system by representing numerous internal nodes' physical displacement DOFs with a smaller number of system-wide modal DOF, greatly reducing the computational cost of simulations. Details of the general method are described below, while further details can be found at [13, 12]. The HCB method is implemented using Abaqus's built-in substructure generation tool [14].

A model's equation of motion, neglecting damping, can be seen below.

$$\mathbf{M}\ddot{\mathbf{x}} + \mathbf{K}\mathbf{x} + \mathbf{F}_J(\mathbf{x}, \theta) = \mathbf{F}_p \tag{1}$$

The nonlinear forces in the system are modeled by the function $\mathbf{F}_J(\mathbf{x}, \theta)$, and the external forcing of the system is $\mathbf{F}_p$. The variable $\theta$ captures the prior state of each node: sticking or slipping. From this equation, the HCB method first partitions all matrices, according to boundary and internal nodes, as follows.

$$\begin{bmatrix} \mathbf{M}_{BB} & \mathbf{M}_{BI} \\ \mathbf{M}_{BI} & \mathbf{M}_{II} \end{bmatrix} \begin{Bmatrix} \ddot{\mathbf{x}}_\mathbf{B} \\ \ddot{\mathbf{x}}_\mathbf{I} \end{Bmatrix} + \begin{bmatrix} \mathbf{K}_{BB} & \mathbf{K}_{BI} \\ \mathbf{K}_{BI} & \mathbf{K}_{II} \end{bmatrix} \begin{Bmatrix} \mathbf{x}_B \\ \mathbf{x}_I \end{Bmatrix} + \begin{Bmatrix} \mathbf{F}_J(\mathbf{x}, \theta) \\ 0 \end{Bmatrix} = \begin{Bmatrix} \mathbf{F}_B \\ \mathbf{F}_I \end{Bmatrix} \tag{2}$$

where $B$ is for boundary DOF, and $I$ is for internal DOF. The internal nodes' coordinates are then converted to modal coordinates, which allows higher frequency modes to be discarded. A transformation between these two coordinate systems is then

generated, as seen below.

$$\begin{Bmatrix} \mathbf{x}_B \\ \mathbf{x}_I \end{Bmatrix} = \mathbf{T}^{HCB} \begin{Bmatrix} \mathbf{x}_B \\ \mathbf{q}_m \end{Bmatrix} = \begin{bmatrix} \mathbf{I} & \mathbf{0} \\ \mathbf{\Psi} & \mathbf{\Phi} \end{bmatrix} \begin{Bmatrix} \mathbf{x}_B \\ \mathbf{q}_m \end{Bmatrix} \tag{3}$$

where $\mathbf{q}_m$ is the reduced set of modal coordinates that approximate the displacements $\mathbf{x}_I$, $\mathbf{I}$ is the identity matrix, $\mathbf{\Psi}$ and $\mathbf{\Phi}$ are the transformation sub-matrices responsible for the coordinate change. The transformed system contains all of the interface DOF but the number of internal DOF is reduced to typically tens of fixed interface modal DOF.

## 2.2 Quasi-Static Modal Analysis

The process of QSMA is described below. For further details, see [11, 4].

Consider the previous equation of motion with $\mathbf{F}_p = \mathbf{F}_{ext} + \mathbf{F}_{pre}$, or the sum of the externally applied force and the preload force. It is assumed that the force in the joints behaves linearly at small amplitudes. In this case, the nonlinear term in the previous equation can be approximated as $\mathbf{K}_0\mathbf{x} \approx \mathbf{F}_J(\mathbf{x}, \dot{\mathbf{x}})$ at small amplitudes. One can then solve the following eigenvalue problem to find the modes for this small amplitude state.

$$\left(\mathbf{K} + \mathbf{K}_0 - \omega_r^2 \mathbf{M}\right) \boldsymbol{\phi}_r = \mathbf{0} \tag{4}$$

Where $\omega_r$ and $\phi_r$ are the respective natural frequency and mode shape of the $r$th mode. Note that the modes thus found are for displacements relative to the preloaded state, yet the model tracks quasi-static displacement starting before the preload is applied. So, when a preload force is applied (as in the case of the unreduced FE truth model) then one must subtract off the preload deflections to relate the quasi-static motions to the modes. A quasi-static load is then applied in the shape of the mode of interest using the mode's eigenvector as follows,

$$\mathbf{K}\mathbf{x} + \mathbf{F}_J(\mathbf{x}, \dot{\mathbf{x}}) = \left(\boldsymbol{\phi}_r^{L,m}\right)^{\mathrm{T}} \alpha \tag{5}$$

where $\boldsymbol{\phi}_r^{L,m}$ is the $r$th row of the pseudo-inverse of $\boldsymbol{\phi}$, computed using the first $m$ modes, and $\alpha$ is a scaling factor that sets the amplitude of the force applied to mode $r$.

Applying this load quasi-statically results in a nonlinear force-displacement curve. This backbone curve is then used to generate a full hysteretic loop using Masing's rules, as shown in Fig. 1 [4]. As is mentioned in [11, 4], the backbone curve and hysteresis loop can then be used to calculate the natural frequency and damping of the structure as a function of vibration amplitude. A typical result is shown in Fig. 9, which is discussed later.

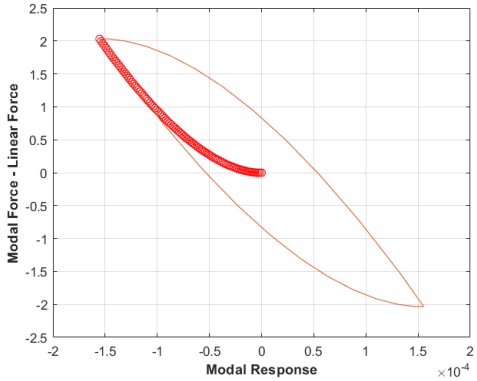


Figure 1: Hysteresis loop generated by applying Masing's rules to the force-displacement backbone curve generated from QSMA.

## 2.3 Four parameter Iwan Elements

This work models the joint's nonlinear behavior using Segalman's four-parameter Iwan element [5], so this defines the joint force $\mathbf{F}_J(\mathbf{x}, \dot{\mathbf{x}})$. Further details regarding how Iwan elements are implemented and the internal forces computed are given in [15]. The Iwan element is a simple and relatively easy to use model that effectively captures power-law energy dissipation due to microslip, and this type of behavior has been observed in several structures with bolted joints [16, 17, 18].

# 3 Case Study: Stacked Beam

Due to its simplicity, a two-dimensional finite element model was chosen as the benchmark for comparing MPC types. This allowed for dynamic analysis to be performed on the model to verify the results obtained from the full-order model QSMA.

The model consists of two cantilever beams stacked on top of each other and bolted together near their free ends, as shown in Fig. 2. Each beam is 8 inches long and 0.25 inches thick. The model was meshed with plane strain elements, which assume that the beam is infinite in width. A pressure load of 212 foot-pounds spanning over 0.25 inches was first applied on the upper surface of the top beam and the lower surface of the bottom beam, seen in the purple region of Fig. 2. This ensured that the beams were in a preloaded state before any further analysis. For a more in depth description of the model, see [11].

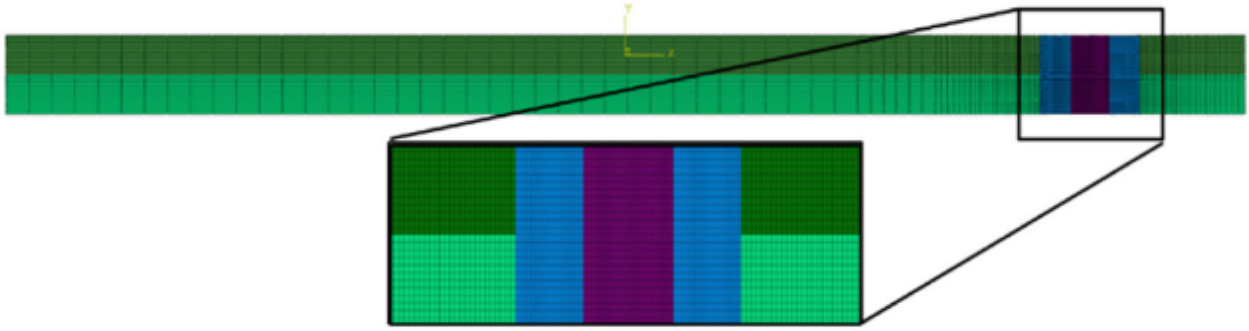

Figure 2: Visual representation of the stacked beam model used to compare MPCs. The magnified section illustrates the pressure load that simulated the bolt load that joins the two beams. The purple region is where the contact pressure is applied, while the blue represents the region with a refined mesh so that contact can be captured accurately.

## 3.1 Application of Quasi-Static Modal Analysis (QSMA) to Truth Model

Simulated measurements were obtained from the full order truth model using QSMA. This provides the relationship between the effective natural frequency and effective damping ratio as a function of the modal acceleration amplitude. QSMA was applied to the model using quasi-static analysis in Abaqus. After applying a pressure load to the model, as discussed in the previous section, Abaqus's eigensolver was used to calculate the linear frequencies and mode shapes of the model, as seen in Table 1 and Fig. 3. The beam has several low order modes, with about every other mode exhibiting clapping of the beams. Shearing of the joint causes a typical bolted-joint type nonlinearity, and Mode 1 is the first mode that exhibits this, so it is the focus of the nonlinear analysis. Hence, Mode 1 was used to calculate the forces in Eq. (5). An Abaqus input file was created to apply this load using a static analysis following the preload step.

Table 1: Preloaded Natural frequencies of the full order Truth model for the first seven modes.

| Mode Number | Frequency |
|---|---|
| 1 | 198.33 Hz |
| 2 | 1035.8 Hz |
| 3 | 1157.4 Hz |
| 4 | 2531.6 Hz |
| 5 | 3177.7 Hz |
| 6 | 4716.6 Hz |
| 7 | 6145.4 Hz |

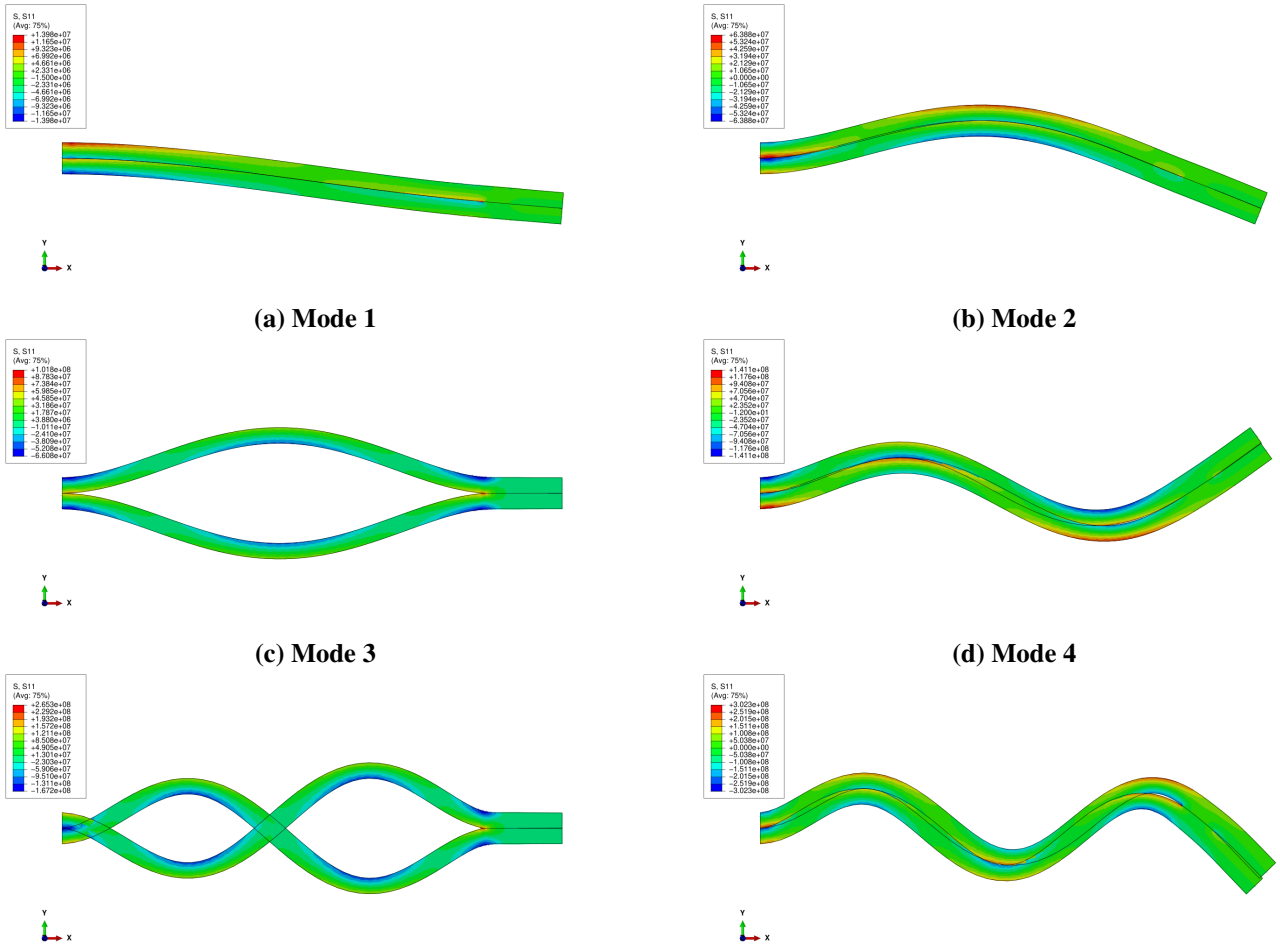

**(a) Mode 1** **(b) Mode 2**

**(c) Mode 3** **(d) Mode 4**

**(e) Mode 5** **(f) Mode 6**

Figure 3: The beam's first six linear modes. Mode 7, which is also referenced in this work, is a higher order clapping mode similar to modes 3 and 5. Modes 1, 2, 4, and 6 are referred to as bending modes, while modes 3, 5, and 7 are referred to as clapping modes. The coloring on the beams shows the x-direction stress, which induces tangential forces in the contact region.

The results from this static analysis were extracted from Abaqus using a Python script, which translated the data into a format suitable for further processing in MATLAB. The first mode's data, shown in Fig. 3, was then used to generate a force-displacement backbone curve after subtracting any linear displacements [11]. Masing's rules were then applied to this backbone curve to generate a hysteresis loop, as seen in Fig. 1. The amplitude-dependent frequency and damping were then calculated using the secant of the backbone curve and the area enclosed in the hysteresis loop [11, 4]. The results of this post-processing can be seen in Fig. 4. Note that the waviness in the damping of the truth model is thought to be caused by the finite size of the mesh and is not physically meaningful.

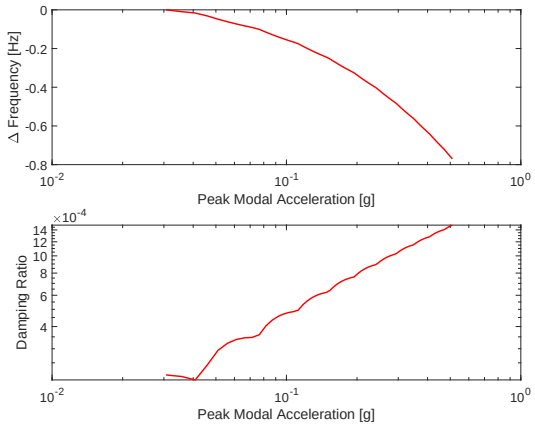


Figure 4: Nonlinear natural frequency and damping generated by running QSMA on the full order model.

This processed data served as our "truth" model. As discussed below, the information from the QSMA analysis of the full-order model will be used during the model updating phase, where optimization methods will be applied to fit linear springs and an Iwan element into our reduced-order model (ROM) to match the results from linear modal analysis and QSMA.

## 3.2 Creating and Calibrating Reduced Order Models

With the truth data in hand, a reduced version of the model was next created using the methods mentioned previously. While in reality the reduced model would likely be created from a model with a coarser mesh and less geometric detail, in this case the ROM was created by simply reducing the truth model.

After meshing the model, two additional unattached nodes were created at the center of the region where the pressure load is applied. These nodes serve as the parent nodes for the MPCs and were attached to a radial subset of joint interface nodes, using Abaqus's *coupling constraints* [14], as illustrated in Fig. 5. The nominal radius of this constraint initially matched the radius of the pressure load, although other radii were also considered, as elaborated later. After selecting the control nodes and radius, one must also select the constraint type: kinematic (RBE2 or RBAR) or continuum distributed (RBE3).

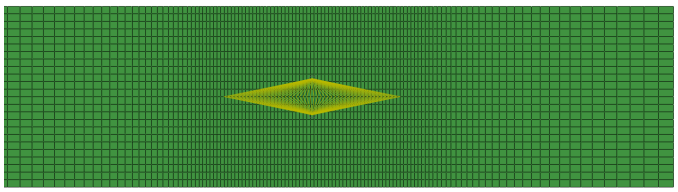

Figure 5: Visualization of MPCs defined on the Stacked Beam Model. Control nodes offset for MPC visibility.

The kinematic method in effect inserts rigid bars between the parent node and the interface nodes, creating a rigid surface. In contrast, continuum distributed constraints use an averaging approach with a specified polynomial (Uniform, Linear, Quadratic, or Cubic) that is used to distribute the forces and moments from the parent node to the child nodes. Thus, Abaqus offers five types of MPCs for users to define. For simplicity, sections 3.3-3.4 will focus on the results obtained using kinematic constraints. Section 4.1 will then show how the results differed when using each of the other types of constraints.

After defining the MPC, Abaqus was used to reduce the system using the HCB method, using the spider parent nodes as the interface nodes. This process reduced the system from approximately 9,000 degrees of freedom, to 26, with three degrees of freedom for each interface node and twenty degrees of freedom for fixed interface modes that were retained during the HCB reduction. The reduced mass and stiffness matrices were then exported from Abaqus into MATLAB, where optimization was used to match the ROM to the simulated measurements from the truth model.

### 3.3 Linear Optimization and Validation

Before inserting an Iwan element into the model, linear springs were inserted to capture the stiffness of the joint for small displacements where no micro-slip occurs. The linear spring in the slip direction will eventually be replaced by an Iwan element, with the linear spring stiffness becoming the $K_T$ parameter of the Iwan element, as will be discussed later. This spring will be referred to as the $K_T$ spring or the slip direction spring in later sections.

The natural frequencies obtained from linear modal analysis of the preloaded, full-order model are taken as known values, as if they had been measured in a modal test. Then, optimization is used to find the linear spring stiffnesses that cause the natural frequencies of the ROM to match those of the truth model as well as possible. This is achieved using a slightly modified version of Matlab's built-in "fminsearch" function, which includes bounds on the search space to speed up optimization convergence and prevent negative stiffness outputs. Because the $K_T$ spring plays such an important role in the nonlinear optimization, it was treated as a parameter and results were obtained for many different values of $K_T$ while the stiffnesses of the other springs were optimized to minimize the errors in the first seven mode frequencies. As an example, Table 2 shows the natural frequencies of the truth model, those of the reduced model, and the percent errors when $K_T = 10^7$ lb/in and optimization was used to find the other spring constants.

Table 2: Natural Frequencies found after Linear Optimization with $K_T$ set to $10^7$ lb/in. The spring constants obtained for the other DOFs were $1.22 * 10^{11}$ lb/in and $8.86 * 10^5$ lb/in for the $y$ translation and $z$ rotation DOFs respectively

| Mode Number | Truth Model Frequency | Reduced Model Frequency | Reduced Model Percent Error |
|---|---|---|---|
| 1 | 198.33 Hz | 196.57 Hz | -0.89% |
| 2 | 1035.8 Hz | 1028.7 Hz | -0.68% |
| 3 | 1157.4 Hz | 1161.3 Hz | 0.33% |
| 4 | 2531.6 Hz | 2527.0 Hz | -0.18% |
| 5 | 4716.6 Hz | 3180.1 Hz | 0.075% |
| 6 | 6145.4 Hz | 6127.5 Hz | -0.29% |

### 3.4 Application of an Iwan Element

To capture the nonlinear behavior of the system, the tangential linear spring was replaced by an Iwan element between the two virtual nodes from the HCB reduction. This substitution enables the model to capture the effects of slip at the interface while maintaining linear behavior in the non-tangential degrees of freedom.

As mentioned in Section 2.3, the Iwan element has four parameters that govern its behavior. A Monte-Carlo optimization was used to find the parameters that brought the nonlinear behavior of the ROM into agreement with the simulated measurements from the truth model. In essence, QSMA is applied to the ROM and the natural frequency and damping are computed over a range of acceleration amplitudes. These are then compared with those from the full-order model. This computation is very fast on the ROM because of its low order. Hence, the optimization algorithm can vary these parameters and search for those that minimize the difference between the ROM and the truth model. An example of such a comparison is shown in Fig. 9. An error metric is computed as the sum of the area between the frequency curves, multiplied by a weighting factor, plus the area between the damping curves [4]. The optimization seeks to minimize this error metric.

## 4 Results

When considering the linear natural frequencies of the structure, the coupling type and MPC radius were found to influence the accuracy of the ROM. These factors are considered in the next two subsections. These results revealed that the optimization drives the slip direction spring stiffnesses excessively high if only the linear modes are considered, and this degrades the model's ability to capture the nonlinear response. This is explored in Sec. 4.3.

### 4.1 MPC Type Impact on Linear Accuracy

Figure 6 explores the effect of the spider type on the accuracy of the linear natural frequencies. Each line shows the percent error in each mode frequency after optimization was used to find the spring constants that minimized the sum of the squared errors of these mode frequencies. The spider types considered are kinematic (RBE2) and continuum distributed (RBE3), with

the latter comprised of uniform, linear, quadratic, and cubic subtypes. The distributed coupling subtypes significantly effect modes 3, 5, and 7, all of which are clapping modes, while minimally affecting the bending modes. Of those, the spiders that use uniform weighting gave the smallest errors in the clapping modes. Therefore, subsequent tests only report on the uniform continuum distributed coupling type.

As seen in Fig. 6, the kinematic (RBE2) spiders produced lower errors than the continuum distributed (RBE3) spiders. However, one should note that the spider area used for this comparison, the "Plus 12" case, turned out to be optimal for the RBE2 spiders and a larger area was needed for RBE3 spiders. This is elaborated in the next subsection.

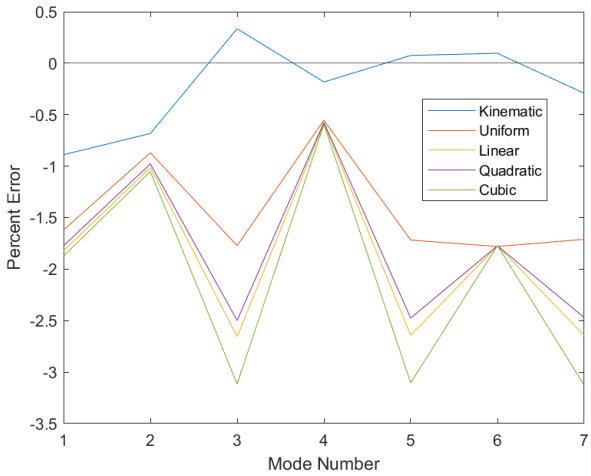


Figure 6: Percent error between the frequencies calculated using the truth model and the ROM. All models used the "Plus 12" spider area, which is explained in Sec. 4.2. The kinematic (RBE2) model uses a rigid spider, whereas the others are continuum distributing (RBE3) spiders with the distribution type (Uniform, Linear, Quadratic, Cubic) listed in the legend.

## 4.2 The Influence of Spider Radius

To explore the effect of the spider radius, models with various spider radii were created and the optimization process was repeated for each. The spider radius initially included only the area directly under the pressure load, or the region shown in purple in Fig. 2. The additional spider radii were denoted "Plus $\alpha$", where $\alpha$ is the number of additional child nodes added on each side of the spider. The radii considered ranged from "Plus 0" to "Plus 49." The latter covered the entire region where contact was defined, which extended from the center of the bolt to the right edge of the beam in Fig. 2 and an equal distance in the opposite direction.

As shown in Fig. 7, the spider radius significantly influences the clapping mode errors and, to a lesser extent, the lower-frequency bending modes. For the Kinematic (RBE2) spiders, the optimal area was the "Plus 12" case, but the "Plus 6" and "Plus 18" models also give good results. The "Plus 12" case corresponds to a $25.3^\circ$ bolt frustum. Interestingly, this lies within the $25 - 33^\circ$ bolt frustum range mentioned by Shigley [19].

In contrast, when uniform continuum distributing (RBE3) type spiders were used, the best results were obtained when a much larger area was used, such as "Plus 30" or "Plus 49." Also, none of the RBE3 cases were able to achieve errors less than $1\%$ for all seven modes, while the best result with kinematic spiders did.

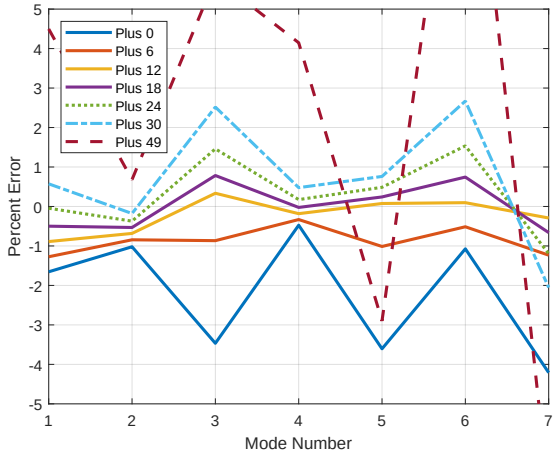


(a) Relationship between radius and modal percent errors of the system for the kinematic (RBE2) coupling type.

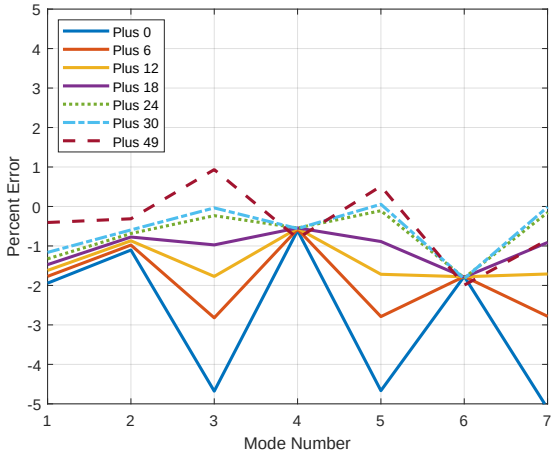


(b) Relationship between radius and modal percent errors of the system for the uniform continuum distributed (RBE3) coupling type.

Figure 7: The effect of MPC radius on the percent errors in the first seven linear natural frequencies. In the "Plus 0" case the spider area is the purple region in Fig. 2 while the "Plus 49" case covered the entire contact region.

## 4.3 Influence of $K_T$ Values on ROM Accuracy

In the course of the optimization it was discovered that the optimizer tended to drive the tangential spring stiffness, which becomes $K_T$ in the Iwan element, to very large values. This was found to adversely affect the nonlinear optimization. Furthermore, the optimizer does this even though there may be a minimal improvement in the correlation between the linear natural frequencies of the ROM and those of the truth model. To study this, the linear optimization was modified by selecting a value for $K_T$ and then optimizing to find the other two spring constants. (In all previous cases the optimizer was allowed to vary all of the spring stiffnesses, including $K_T$). Then the $K_T$ value was varied to see how it affects the linear natural frequencies; the results are shown in Fig. 8. Then, the spring constants found in that step were used in a nonlinear optimization. The nonlinear optimization compared the frequency and damping versus amplitude predicted by QSMA with those of the truth model, shown in Fig. 4, and adjusted the Iwan parameters until the best possible agreement was obtained.

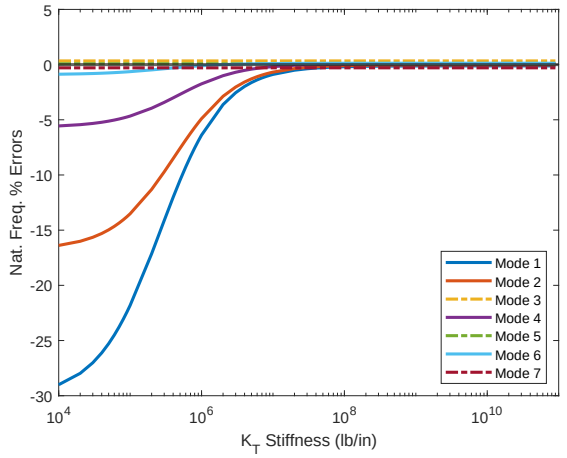


(a) Percent errors in the linear mode frequencies as $K_T$ stiffness was varied. Clapping modes marked with dash-dot lines.

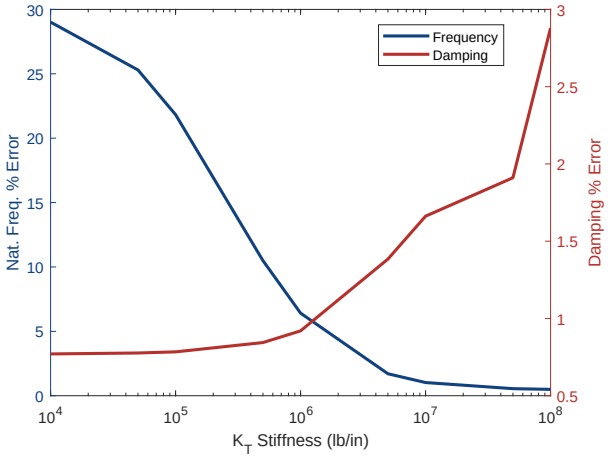


(b) Relationship between $K_T$ stiffness and the average percent error in the nonlinear frequency and damping of Mode 1.

Figure 8: Effects of $K_T$ stiffness on ROM accuracy. These results used the model with kinematic (RBE2) spiders and with the "Plus 12" spider area.

All of the results shown in Fig. 8 used Kinematic (RBE2) spiders and the "Plus 12" spider area. Figure 8a shows the percent

errors in the natural frequencies as $K_T$ was varied. Increasing the linear spring stiffness in the slip direction reduces the percent errors in the bending modes (Modes 1, 2 and 4), although with diminishing returns. The frequencies of the clapping modes are small in all cases. The error in Mode 1 falls below $1.0\%$ for $K_T > 8 \times 10^6$.

Figure 8b shows the results of the nonlinear optimization step. The optimization, which was repeated for each value of $K_T$, produced an estimate of the natural frequency and damping of Mode 1 as a function of vibration amplitude. These were then compared to those of the truth model, shown in Fig. 4. (An example of this comparison is shown in Fig. 9 for $K_T = 10^6$ lb/in.) For each value of $K_T$, the average percent error was computed and is shown in Fig. 8b for both the damping and natural frequency. These results show that the nonlinear damping increases in error as $K_T$ increases beyond about $10^5$ or $10^6$ lb/in. In contrast, the error in the Mode 1 natural frequency increases for $K_T < 10^6$, primarily because its linear mode frequency becomes much less accurate. Both objectives must be considered to obtain a model that captures both the natural frequencies and the damping. The model captures amplitude dependent frequency and damping of the truth model very well.

Results of roughly similar quality were obtainable for values of $K_T$ near the optimium value, but the results showed considerable error for $K_T > 10^8$ lb/in, and even more so for $K_T > 5 * 10^8$ lb/in. At higher $K_T$ values, less energy goes into the Iwan element, so the damping in the ROM becomes much lower than that of the target. As a result, the optimization algorithm drives the slip force $F_s$ to smaller and smaller values until macro-slip happens in the range shown in Fig. 9, where the response should be purely micro-slip. Singh et al. [9] observed similar issues, although in their study the value of $K_T$ seemed to be dictated by the spider type, with RBE2 spiders producing smaller values of $K_T$ and RBE3 spiders producing larger values. The approach presented here, in which $K_T$ is treated as a parameter rather than as an optimization variable, seems to simplify the optimization process while providing the user with a clear picture of any tradeoffs that must be made.

## 4.4 Optimal Results

Among all of the case studies considered, the best results were obtained with kinematic (RBE2) coupling with a spider radius of "Plus 12." The optimal value of $K_T$ was found to be $10^6$ lb/in. Table 3 compares the linear natural frequencies of the ROM when these settings are used to the frequencies generated using the truth model. The linear natural frequencies are less accurate than those presented in Sec. 4.2, where optimization was performed considering only the linear natural frequencies. When that was done the errors were less than $1\%$ for most modes, while this ROM has errors of errors of $-6.4\%$ and $-4.9\%$ for Modes 1 and 2 respectively. However, this model gave an excellent fit for the nonlinear frequency and damping of the joint, which are shown in Fig. 9. Note that the frequency error in Fig. 9 is expressed as the change in the frequency from its linear value, so as to focus on how the model captures the nonlinearity and not on the error in the linear natural frequency. In contrast, if the $K_T$ values found in Sec. 4.2 were used in the nonlinear model, the error in nonlinear frequency and damping would be much more significant.

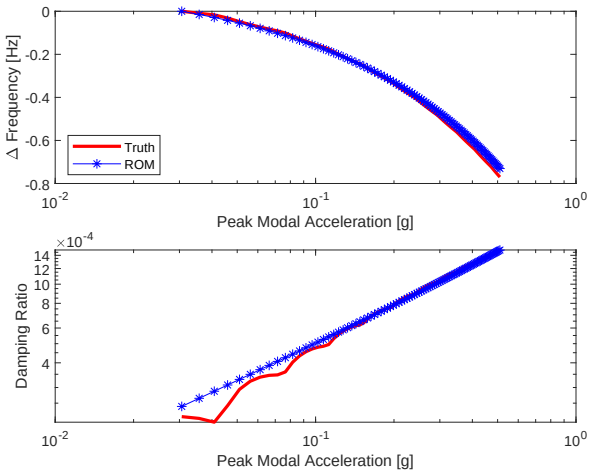


Figure 9: Comparison of nonlinear frequency and damping versus vibration amplitude between the full-order truth model and the best ROM (Kinematic, "Plus 12," $K_T = 10^6$ lb/in).

Results were also generated using the continuum distributed (RBE3) spider type with a uniform forcing distribution. This model used a "Plus 30" spider radius and a $10^6$ lb/in $K_T$ stiffness. This value is once again smaller than the optimum used in Sec. 4.2. It was found that the ROM with this MPC type was also able to accurately capture the nonlinear frequency and damping of

Mode 1. The frequency and damping curves obtained with this ROM are nearly indistinguishable from those in Figure 9 so they are not repeated here. However, as was the case with the RBE2 spiders, using $K_T = 10^6$ increased the errors in the linear mode frequencies. Table 3 shows that the model with RBE3 spiders also had errors up to $6.5\%$, significantly increased as compared to the best results obtained in Sec. 4.2.

Table 3: Linear natural frequencies calculated using two models with different MPC types. One model consisted of a kinematic (RBE2) spider with a "Plus 12" radius. The other model utilized a continuous distributed (RBE3) spider with uniform forcing distribution and a "Plus 30" radius. Both models used a $K_T = 10^6$ lb/in.

| Mode # | Truth Model Freq. (Hz) | Kinematic (RBE2) Freq. (Hz) | Continuum (RBE3) Freq. (Hz) | RBE2 % Error | RBE3 % Error |
|---|---|---|---|---|---|
| 1 | 198.33 | 185.67 | 185.34 | -6.4 | -6.5 |
| 2 | 1035.8 | 985.09 | 985.8 | -4.9 | -4.8 |
| 3 | 1157.4 | 1161.3 | 1157 | 0.33 | -0.036 |
| 4 | 2531.6 | 2487.5 | 2474.3 | -1.7 | -2.3 |
| 5 | 3177.7 | 3180.1 | 3179.5 | 0.074 | 0.056 |
| 6 | 4716.6 | 4711.8 | 4618.2 | -0.10 | -2.1 |
| 7 | 6145.4 | 6127.4 | 6144.6 | -0.29 | -0.014 |

# 5 Conclusion

This paper has presented the first efforts at using spidering, Hurty/Craig-Bampton reduction, linear springs, and an Iwan element to capture the micro-slip damping and nonlinear behavior of a simple two dimensional structure. The structure is simple and computationally efficient, allowing a large range of simulations to be performed and many optimization case studies. The end goal of the work is to use this benchmark system to understand the limitations of this type of modeling. The effort so far has confirmed the findings in other studies, namely the importance of the value of the tangential stiffness $K_T$ on the ability of the nonlinear model to capture the damping in the joint. While a prior study [9] found that Kinematic or RBE2 spiders produced much smaller values of $K_T$ than continuum distributing spiders (RBE3), this work found that each spider type can obtain reasonable results if the spider area is varied. If $K_T$ was allowed to be large enough then either model could reproduce the natural frequencies of the first seven modes with less than $1\%$ error. However, with the large values of $K_T$ that were required, the model could not capture the nonlinear damping accurately.

To address this, the authors modified the optimization approach relative to that used in prior works. In those studies [4, 9], optimization was used to find the spring constants of a set of springs that define the joint stiffness, and one of those springs was then replaced with an Iwan element. In this work, the stiffness of the Iwan element was treated as a parameter that was varied to reveal its effect on both the linear natural frequencies of the assembly and on the nonlinear frequency and damping of a mode of interest. Using this approach, it was relatively straightforward to identify a model that obtained a reasonable trade-off between error in the linear mode frequencies and error in the capturing the nonlinearity.

It is interesting to note that the best result that was obtained did not meet the standard that is typically enforced in the aerospace industry [2, 20]. Specifically, the first and second modes were not within the $< 3\%$ or $< 5\%$ frequency error standards. This was true for either RBE2 or RBE3 spiders. It is surprising that better results could not be obtained for such a simple system, and this is a subject of ongoing study. On the other hand, the model did accurately capture the nonlinear damping of the structure due to friction, a feat that has rarely been achieved for bolted structures, and such a model could still prove useful in various settings.

The authors hope to continue to study this model, including the occurrence of mode coupling, as initiated by Singh et al. [21], to understand the conditions under which a ROM such as this can capture these effects.

# References


[1] James P. Winkel, Vicente J. Suarez, and James C. Akers. Combined Qualification Vibration Testing and Fixed Base Modal Testing Utilizing a Fixed Based Correction Method. Orlando, FL, 2020.

[2] USAF. Military Handbook 340A: Test Requirements for Launch, Upper-Stage, and Space Vehicles, Vol I : Baselines, (MIL-HDBK-340A), United States Air Force. Technical report, 1999.

[3] Matt Griebel, Jesse Wilson, Adam Johnson, Brent Erickson, Andrew Doan, Chris Flanigan, Paul Bremner, Joel Sills, and Erica Bruno. Orion E-STA Nonlinear Dynamic Correlation and Coupled Loads Analysis. El Segundo, CA, June 2019. Matt Griebel, Jesse Wilson, Adam Johnson, Brent Erickson, Andrew Doan, and Chris Flanigan, Quartus Engineering, Inc., Paul Bremner, AeroHydroPLUS, Joel Sills, NASA Engineering Safety Center, Erica Bruno, Analytical Mechanics Associates, In.

[4] Robert M. Lacayo and Matthew S. Allen. Updating Structural Models Containing Nonlinear Iwan Joints Using Quasi-Static Modal Analysis. *Mechanical Systems and Signal Processing*, 118(1 March 2019):133–157, 2019. Number: 1 March 2019.

[5] Daniel J. Segalman. A Four-Parameter Iwan Model for Lap-Type Joints. *Journal of Applied Mechanics*, 72(5):752–760, February 2005.

[6] D. J. Segalman, D. L. Gregory, Michael J. Starr, Brian R. Resor, Micheal D. Jew, James P. Lauffer, and Nicoli M. Ames. Handbook on Dynamics of Jointed Structures. Technical report, Sandia National Laboratories, Albuquerque, NM 87185, 2009.

[7] Matthew S. Allen, Robert Lacayo, and Matthew R.W. Brake. Quasi-static Modal Analysis based on Implicit Condensation for Structures with Nonlinear Joints. September 2016.

[8] Matthew R. Brake, Pascal Reuss, Daniel J. Segalman, and Lothar Gaul. Variability and Repeatability of Jointed Structures with Frictional Interfaces. In Matt Allen, Randy Mayes, and Daniel Rixen, editors, *Dynamics of Coupled Structures, Volume 1*, Conference Proceedings of the Society for Experimental Mechanics Series, pages 245–252. Springer International Publishing, 2014.

[9] Aabhas Singh, Wall, Mitchell, Allen, Matthew S., and Kuether, Robert J. Spider Configurations for Models with Discrete Iwan Elements. In *Nonlinear Structures and Systems*, volume 1, pages 25–38, Orlando, Florida, January 2019. Springer.

[10] A. Singh, M. Scapolan, Y. Saito, M. S. Allen, D. Roettgen, B. Pacini, and R. J. Kuether. Experimental Characterization of a new Benchmark Structure for Prediction of Damping Nonlinearity. Orlando, Florida, 2018.

[11] Emily Jewell, Matthew S. Allen, Iman Zare, and Mitchell Wall. Application of Quasi-Static Modal Analysis to a Finite Element Model and Experimental Correlation. *Journal of Sound and Vibration*, 479(4 August):115376, 2020. Number: 4 August.

[12] W. C. Hurty. Dynamic analysis of structural systems using component modes. *AIAA Journal*, 3(4):678–685, April 1965. Number: 4.

[13] R.R. Jr. Craig and M.C.C. Bampton. Coupling of Substructures for Dynamic Analysis. *AIAA Journal*, 6(7):1313–1319, 1968. Number: 7.

[14] Abaqus analysis user's guide, 2023.

[15] Drithi Shetty and Matthew S Allen. A General Iwan Element Derived from Quasi-Static Force-Displacement Data. In *39th International Modal Analysis Conference (IMAC XXXIX)*, page 9, Orlando, FL, February 2021.

[16] Daniel R. Roettgen and Matthew S. Allen. Nonlinear characterization of a bolted, industrial structure using a modal framework. *Mechanical Systems and Signal Processing*, 84:152–170, 2017.

[17] Brandon Deaner, Matthew S. Allen, Michael J. Starr, D. J. Segalman, and Hartono Sumali. Application of Viscous and Iwan Modal Damping Models to Experimental Measurements From Bolted Structures. *ASME Journal of Vibrations and Acoustics*, 137:12, 2015.

[18] Mitchell P. J. Wall, Allen Allen, Matthew S, and Robert J. Kuether. Observations of Modal Coupling due to Bolted Joints in an Experimental Benchmark Structure. *Mechanical Systems and Signal Processing*, 162:107968, 2022.

[19] Richard Gordon Budynas and J. Keith Nisbett. *Shigley's Mechanical Engineering Design*, volume 9. McGraw-Hill, New York, 2011.

[20] NASA. Loads Analysis of Spacecraft and Payloads. Standard NASA-STD-5002A, National Aeronautics and Space Administration (NASA), USA, 2019.

[21] Singh, Aabhas, Allen, Matthew S., and Kuether, Robert J. Multi-mode Quasi-static Excitation for Systems with Nonlinear Joints. *Mechanical Systems and Signal Processing*, Vol. 185(15 February):109601, 2023.